Materials Science and Engineering A 528 (2011) 1694–1701

Contents lists available at ScienceDirect

Materials Science and Engineering A

journal homepage: www.elsevier.com/locate/msea

Theory for the failure stress of a quasi-equilibrium, brittle polycrystal with a small void fraction

Robert S. Farr[a,b,*], Aitor Luque[c], Andrew Hoddle[d]

[a] Unilever R&D, Olivier van Noortlaan 120, AT3133 Vlaardingen, The Netherlands
[b] The London Institiute for Mathematical Sciences, 22 S. Audley St., Mayfair, London, UK
[c] CEIT and Tecnun (University of Navarra), Manuel de Lardizabal, 15, 20018 San Sebastián, Spain
[d] Unilever CoE Ice Foods, Colworth House, Sharnbrook, Bedford MK44 1LQ, UK

ARTICLE INFO

Article history:
Received 22 May 2010
Received in revised form 27 October 2010
Accepted 27 October 2010

PACS:
81.10.Aj
62.20.M–

Keywords:
Fracture
Size effects
Polydispersity
Theory

ABSTRACT

An equilibrated polycrystalline material is considered, containing a small fraction of void space (melt or vapor), for which the crystals are above their roughening transition against this medium. The grain boundaries are approximated to have equal free energy per unit area, so that they assume the geometry of lamellae in a dry foam. It is argued that the void space of the polycrystal consists of sharp-edged cavities of tetrahedral symmetry at the grain vertices, and universal shapes for these voids are calculated. Treating these voids as incipient fractures, a general analytic expression for the failure stress (by fracture) of the polycrystal is derived, in terms of void fraction, grain size and polydispersity, fracture toughness and surface and grain boundary free energies. This expression is expected to apply when grains are large enough for fracture to be brittle, and the relation of this mechanism to other modes of material failure, such as plastic yield (as described by the Hall–Petch relation) or breakage under stresses from elastic anisotropy is discussed.

1. Introduction

Polycrystalline materials are abundant in nature: examples include igneous rocks [1], glacial ice [2] and beeswax [3]. They also occur frequently as artificial materials, such as metals, ceramics [4], chocolate [5] and sorbets [6].

Under a sufficiently strong applied stress, a void-free polycrystal may eventually yield plastically, as dislocations are nucleated, move through the crystal structure, and encounter grain boundaries. The yield stress σ_Y often obeys the Hall–Petch [7] relation, $\sigma_Y = \sigma_0 + K_{hp}/\sqrt{d}$, where K_{hp} and σ_0 are constants for the particular material and d is the grain diameter. This arises from the movement of dislocations being blocked by grain boundaries, and then accumulating until their mutual repulsions allow them to overcome this energy barrier [7–9].

In addition, material failure can occur via the nucleation and propagation of microcracks, which can lead to brittle behaviour. Such cracks might form by a dislocation pileup mechanism [10] or, if there are microcrack precursors already present (again perhaps from dislocation pileup), they might be made to propagate under the applied stress, or stress concentrations produced by elastic anisotropy [11]. Indeed, for a material such as ice, Gold [12] found two families of cracks: a strain dependent set attributed to dislocation pileup, and a second set associated with brittle behaviour.

The elastic anisotropy mechanism bears further consideration for its contrast to the theory we develop below. If the randomly oriented grains of a polycrystal are elastically anisotropic, then when the material is put under load, the local differences between crystal compliances will lead to inhomogeneities in the stress field. These inhomogeneities will be on a length scale set by the crystal size, and will be present even if the deformation on long length scales is affine [11]. The resulting stresses behave as finite shear forces at the grain boundaries, but also generate stress singularities at jogs on these boundaries, at lines where three grain boundaries meet, and at the points where such grain triple junctions intersect a free surface such as a void [13]. Nevertheless, the singularities encountered are rather weak: a logarithmic divergence (with respect to distance from the singularity) has been found in the case of loading induced by thermal expansion [14], and singularities substantially weaker than the minus one half power (associated with cracks) have been found for mechanical loading [15,13]. This elastic anisotropy mechanism was analysed by Shyam Sunder and Wu [16], who assumed that there are microcrack precursors present (for example from

* Corresponding author at: Unilever R&D, Olivier van Noortlaan 120, AT3133 Vlaardingen, The Netherlands.
E-mail address: robert.farr@unilever.com (R.S. Farr).

0921-5093/$ – see front matter © 2010 Elsevier B.V. All rights reserved.
doi:10.1016/j.msea.2010.10.094

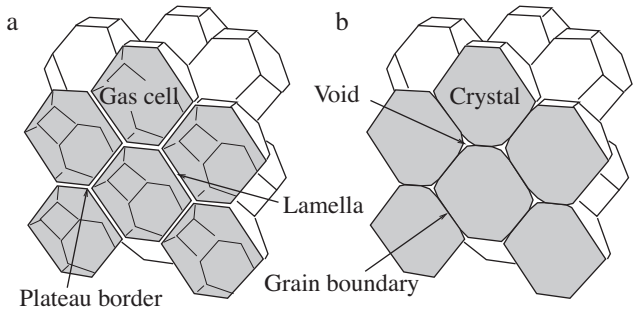

Fig. 1. (a) Schematic of a section through a dry foam, showing gas cells, foam lamellae and Plateau borders. (b) Schematic of a section through a polycrystal with a small void fraction, illustrating its similarity in geometry to an 'inverse' foam.

previous dislocation pileup), and that these precursors have a size which is a fixed fraction of the grain size. These authors then derived a brittle failure criterion, which has an approximate inverse square root grain size dependence, deriving ultimately from the assumption on microcrack precursor length and the Griffith criterion for crack growth [17].

The discussion so far concerns void-free polycrystals, but often during processing, or as a final material, a polycrystal will contain a significant fraction of void space. This is true of sea ice [18], where the incorporated electrolytes prevent complete freezing, and is also the case for magma [19] and many ceramics at elevated temperatures when the material is partially molten. Materials manufactured by high temperature powder sintering [4] usually contain voids filled with air even after cooling, and a similar material structure is encountered under natural conditions in the form of snow [20]. The elastic anisotropy mechanism has been adapted to the case where rounded voids (such as air bubbles) are present [21], and the finite stress concentrations so induced (e.g. a factor of two at the surface of a spherical void) enhance this mechanism and lead to a prediction for how much weaker a porous polycrystal is than its massive counterpart.

In this paper, we take a different approach: we treat the case where voids between the grains have evolved towards a local (quasi-)equilibrium, under the influence of thermodynamic forces. Under the assumption of roughened crystals [22] and equal grain boundary energies per unit area (discussed below), the undeformed structure of a well-equilibrated polycrystal with little void space will be governed by similar structural rules to a dry foam – but with gas cells in the foam having the same shape as the grains of the polycrystal; grain boundaries taking the place of foam lamellae, and the voids in the polycrystal taking the place of the vertices (and potentially the Plateau borders) in the foam. In that sense, we may think of the undeformed polycrystal as analogous to an *inverse* foam, as shown schematically in Fig. 1. This analogy was first made by Smith [27].

If we consider the sharp-edged voids (Fig. 1) as a collection of incipient fractures, then it is clear that another mechanism for material failure can operate in addition to those discussed so far: under suitable loading conditions a fracture (represented initially by a void) will grow, and since the critical stress for this to happen falls with increasing crack size [17], this can lead to a positive feedback and macroscopic failure of the entire sample. This can happen even in the absence of elastic anisotropy, but may be enhanced by stress fields from it.

Under the assumption of roughened crystals and equal grain boundary energies, the voids are of tetrahedral symmetry and have universal shapes which we calculate numerically in Section 3. Using fracture mechanics (Section 4) and recent results on the statistics of random foams (Section 2), we then construct a general theory for the strength of polycrystals with voids. We expect this approximate result to hold down to a void volume fraction at which it exceeds (and is thus cut off by) the Hall–Petch value for a void-free polycrystal, or failure arising from elastic anisotropy or other mechanisms (see for example Ref. [23]).

2. Grain statistics

To begin the analysis, we note that the void geometry is determined by the physics of the crystal interfaces: We assume that all the crystallographic orientations are above the roughening transition [22] against the vapor or melt in the cavities, and that the free energy per unit area of these interfaces is approximately independent of orientation (see for example Ref. [24]) and given by γ. Under these circumstances, the equilibrium shape [25] of an isolated crystal will be a sphere.

In a polycrystal there will be grain boundaries, and where a grain boundary with energy γ_{gb} per unit area meets the surface of a void, local, microscopic equilibrium will rapidly be established, and there will be a notch [26] with dihedral angle θ_0 given, from simple force balance, by

$$2\gamma \cos\left(\frac{\theta_0}{2}\right) = \gamma_{gb}. \tag{1}$$

For the purposes of this paper, we make the simplifying assumption that the grain boundary energy per unit area between any two adjacent grains in the polycrystalline material has the constant value γ_{gb}. Clearly this cannot be true in reality, where there is a range of values corresponding to different degrees of orientational mismatch between the lattices. However, the true population of grain boundary energies (per unit area) will have an average value, and some scatter around this average. Our approximation corresponds to ignoring this scatter.

Under this assumption of equal grain boundary energies per unit area, the structure of an undeformed and well-equilibrated polycrystal with little void space will be governed by the same structural rules as is a dry foam, as illustrated in Fig. 1 and described in Section 1.

The rules governing the structure of a foam were formulated by Plateau [28], and are that in stable systems, the films between gas cells are surfaces of constant mean curvature, which meet in threes with angles of $2\pi/3$ radians between the surfaces at the lines of contact, while these lines of contact meet in fours in a regular tetrahedral arrangement, with angles of $\arccos(-1/3) \approx 1.911$ radians between any two meeting lines.

For a re-crystallizing polycrystal evolving subject to these rules, we expect that there will be at late times an asymptotic structure which becomes coarser over time but for which the statistics of the geometry and topology do not otherwise change. The geometry of such a foam or polycrystal will be specified completely by the number average volume $\langle V \rangle$ of the cells.

A real polycrystal will not necessarily be in this scaling regime, and therefore more parameters are needed in order to identify the statistical properties of its geometry. In the work of Kraynik et al. [29] (who analysed the analogous case of a foam, and whom we follow here) this was done through a polydispersity parameter p, defined by

$$p = \frac{\langle R^3 \rangle^{2/3}}{\langle R^2 \rangle} - 1. \tag{2}$$

In Eq. (2), $\langle \cdot \rangle$ denotes number average, and for a cell with volume V, an effective radius R can be defined through $V = (4/3)\pi R^3$. The parameter $p \geq 0$ vanishes for a monodisperse foam, and for the most polydisperse foams generated in Ref. [29], which have cell volumes ranging over 3 orders of magnitude, $p = 0.47$.

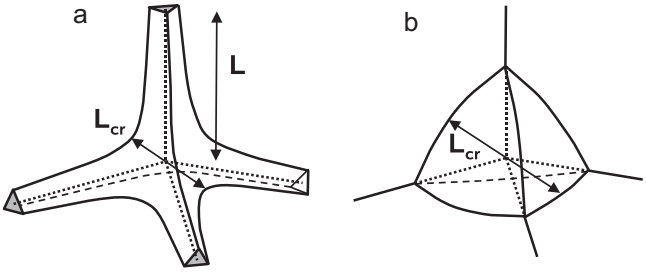

Fig. 2. (a) Shows schematically an open cavity, with 'legs' of length L. This case holds for $\theta_0 < \pi/3$. (b) Shows schematically a closed cavity, which holds for $\theta_0 \geq \pi/3$. In both cases, the symmetry group of the shape is that of a regular tetrahedron.

For the purposes of this paper, we need expressions for the number of vertices N_V per unit volume in the structure, and also the total length of edges L_E per unit volume of the structure. Edges are termed Plateau borders in a foam, but in our case they are the lines where three grain boundaries meet.

We define non-dimensional numbers n_V and l_E to capture this structural information:

$$n_V \equiv \langle V \rangle N_V, \tag{3}$$

$$l_E \equiv \langle V \rangle^{2/3} L_E. \tag{4}$$

From Ref. [29],

$$l_E \approx \frac{5.32}{(1+p)} + 0.063, \tag{5}$$

while the average number of faces per cell is given, from the same source, by

$$\langle F \rangle \approx 13.8 - 9.9p + 10.0p^2, \tag{6}$$

for $p \in (0, 0.47)$.

Using Eq. (6), together with the fact [28] that foam polyhedra are trivalent (so that for each cell, the number of edges is 3/2 times the number of vertices), and Euler's characteristic for polyhedra [30], we find that the number of vertices per cell is twice the number of faces, less 4. Again because of Plateau's rules, each vertex is shared by 4 cells, and so we obtain the estimate [valid for $p \in (0, 0.47)$] of

$$n_V \approx 5.88 - 4.97p + 5.02p^2. \tag{7}$$

Eqs. (5) and (7) are the results we need to proceed.

3. Geometry of the voids

If we now consider a polycrystal with void space, then these voids will have a complex geometry, consisting of curved surfaces where the crystals meet the melt or vapor, and also edges, with a well defined dihedral angle θ_0, occurring where the grain boundaries end at the melt or vapor. We now proceed to analyse the details of this geometry, which for low void fractions depends only on θ_0:

Consider a void in the neighbourhood of a vertex where four crystals meet. From Plateau's rules, the local symmetry around the vertex is that of a regular tetrahedron. The void may have 'legs' as shown in Fig. 2(a), which extend in the four tetrahedral directions. In practice they will extend only as far as the next cavity. However, for the purposes of calculation, it is useful to consider them having some definite length L as in Fig. 2(a). Alternatively, the cavity may be localized around the vertex, as shown in Fig. 2(b).

Which of these two cases obtains, is determined by the dihedral angle. A 'leg', if it exists, must replace three meeting grain boundaries, and be energetically favourable over this configuration. If we assume that the cross section of the leg consists of three circular arcs (shown as solid curves in Fig. 3) and these replace the three

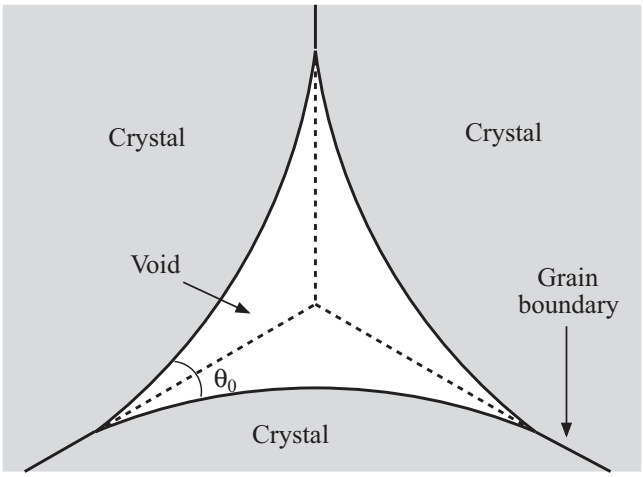

Fig. 3. Section through one of the 'legs' in Fig. 2(a). The curved lines are crystal–void interfaces, which have an energy per unit length of leg given by the length of these curved lines multiplied by γ. The dashed lines are three meeting grain boundaries, which the leg has replaced. These grain boundaries have an energy per unit area of γ_{gb}.

grain boundaries (shown as dashed lines in the same figure), then a short calculation shows that closed, finite cavities will be preferred, provided $\theta_0 > \pi/3$ and open cavities with indefinitely extended legs, provided $\theta_0 < \pi/3$.

In Fig. 2, as well as the length L of the legs, we have defined an effective crack length L_{cr} diagonally across the cavity. Eventually, we will relate these geometrical properties to those of the polycrystal. To do this, we note that, provided the length L of a leg is sufficiently long, the volume v_c of the cavity will be given by

$$v_c = A(\theta_0) L_{cr}^3 + B(\theta_0) L_{cr}^2 L \tag{8}$$

with $B(\theta_0) = 0$ for $\theta_0 > \pi/3$.

In order to obtain our final estimate for the failure stress of a polycrystal, we require expressions for $A(\theta_0)$ and $B(\theta_0)$. These can be obtained by a simple numerical scheme:

The surfaces of the cavities are discretized into triangles, as described in Appendix A. The interfacial energy U_{int} is calculated, relative to the case of a cavity of zero volume, and also the actual volume $\hat{v}$ enclosed by the cavity is calculated. An energy functional

$$U \equiv U_{\text{int}} + \xi(\hat{v} - \hat{v}_0)^2 \hat{v}_0^{-4/3} \tag{9}$$

is then constructed and minimized, where $\hat{v}_0$ is a target volume, and ξ a Lagrange multiplier which penalizes deviations from the target volume and ensures the shape converges to a non-trivial solution.

For the case of an enclosed cavity, a single optimization is required. However, for an open cavity, several calculations, with different values of the leg length L are needed, in order to extract both $A(\theta_0)$ and $B(\theta_0)$.

Examples of initial and final (optimized) cavity shapes for the case of $\theta_0 = 0.6$ are shown in Fig. 4(a) and (b), and for the case of $\theta_0 = 2$ are shown in Fig. 4(c) and (d).

The numerical results for $A(\theta_0)$ and $B(\theta_0)$ are shown in Fig. 5 as open and closed symbols (respectively), for discretization parameters $M = 12$ and $N = 24$ (see Appendix A).

For ease of use, the data can be fitted to the following simple forms (θ_0 being measured in radians): For $\theta_0 < \pi/3$

$$A(\theta_0) \approx 0.07 + 0.016\theta_0 + 0.26\theta_0^2, \tag{10}$$

$$B(\theta_0) \approx 0.174 \left[\left(\frac{\pi}{3} \right)^{3.3} - \theta_0^{3.3} \right], \tag{11}$$

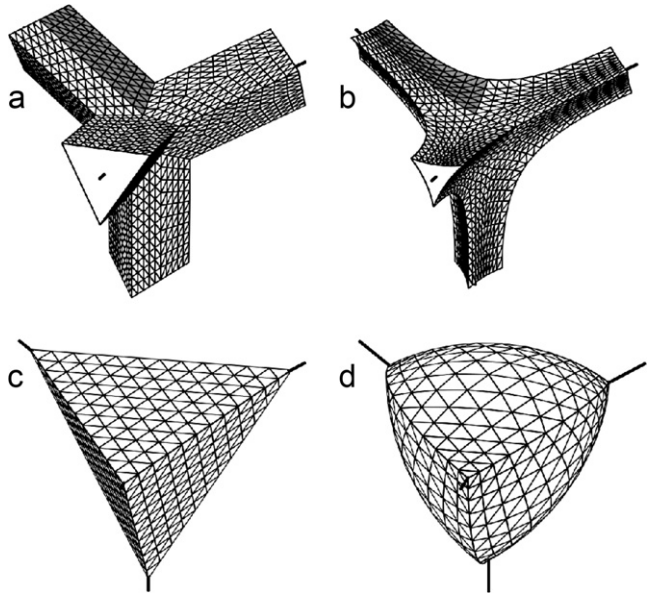

Fig. 4. (a) Initial configuration and (b) final, optimized configuration for the numerical solution to an open cavity shape with $\theta_0 = 0.6$. The surface discretization is as described in Appendix with $M = 5$ and $N = 10$.(c) Initial configuration and (d) final, optimized configuration for a closed cavity with $\theta_0 = 2$ and $N = 12$.

and for $\theta_0 > \pi/3$

$$A(\theta_0) \approx 0.26 + 0.0464\theta_0 + 0.0037\theta_0^3 + 150\exp(-8\theta_0), \quad (12)$$

$$B(\theta_0) = 0. \quad (13)$$

Note that in Eqs. (10)–(13), the functional forms are chosen arbitrarily, and do not reflect an anticipated mathematical structure of the exact solution.

We also note that if the cavities are allowed to come into equilibrium with each other, through the connecting 'legs' (or via pre-melting [4] at the meeting grain boundaries), then the length L_{cr} for all the cavities will tend to become equal, even if there is a distribution of grain sizes.

4. Fracture behaviour

As noted above, the voids, with their sharply notched edges, constitute a collection of incipient cracks. If the material as a whole is subject to a stress field with at least one tensional component σ_∞, then some of these voids will be oriented so that they have a tendency to grow by opening ('mode I' loading). We will assume (due to the weaker exponents of the stress divergences for the other modes near a V-notch [31]) that failure under mode I loading represents the greatest vulnerability to crack growth and sets the failure stress σ_F of the polycrystal under tension. We are therefore interested in the conditions under which a crack at the notch tip will propagate.

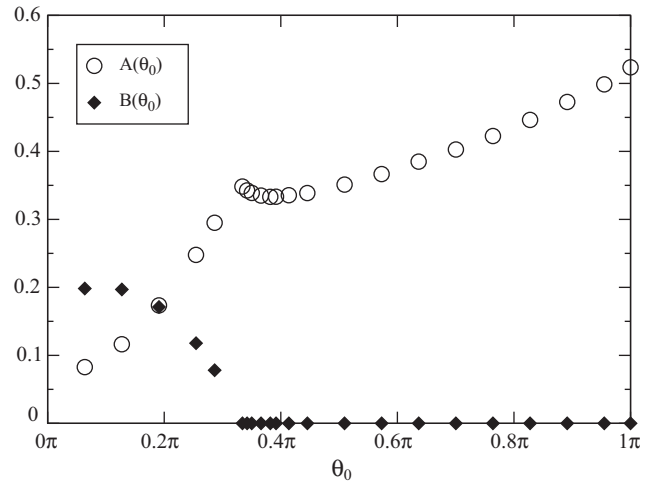

Fig. 5. Numerical values for $A(\theta_0)$ and $B(\theta_0)$, using the discretization described in Appendix with $N = 24$ and (for $\theta_0 < \pi/3$), $M = 12$.

As analysed by Griffith [17], the presence of a true crack (as opposed to a cavity or V-notch) relieves the elastic strain in its neighbourhood, and this neighbourhood extends roughly a distance of the crack size in all directions where material is present. When such a crack grows, the liberated elastic energy is focused down to the crack tip. A simple argument then shows that the crack will grow if

$$\sigma_\infty \gtrsim \left(\frac{EG}{L_{cr}}\right)^{1/2}, \quad (14)$$

where E is the Young modulus and G is the energy (from surface free energy, plastic deformation, etc.) required to create unit area of new crack interface. In Eq. (14) we have omitted a geometry-dependent prefactor. In the case of completely brittle fracture generating a flat crack surface, G would be twice the solid/vapor surface free energy.

Unfortunately, this argument does not immediately generalize to more complex geometries such as V-notches, and leaves unstated the possible relation of G to material properties in any but the simplest case referred to above. To proceed, it has long been recognized that it is necessary to treat the local stress fields: if we consider a V-notch in a linear elastic material, which is subject to mode I loading (opening), then near its tip there will be a divergence in the stress. For example, the principal component of the stress tensor in plane polars (r, θ) a small distance r from the notch tip along the bisector of the notch into the material will to leading order be given by [33,34]

$$\sigma_{\theta\theta} = K_I^N (2\pi r)^{-\lambda}, \quad (15)$$

where K_I^N is the 'notch stress intensity factor' (or 'generalized stress intensity factor'), and the exponent λ (which falls from 0.5 at $\theta_0 = 0$ to 0 at $\theta_0 = \pi$) is given by the smallest positive root [33] of

$$\sin[(\lambda - 1)(2\pi - \theta_0)] = (\lambda - 1)\sin\theta_0. \quad (16)$$

It is useful to have an explicit formula for λ. By treating both θ_0 and $\lambda - 1/2$ as small quantities and taking the first two terms in the Taylor series of Eq. (16), we obtain

$$\lambda \approx \frac{1}{2} - \frac{\theta_0^3}{32\pi} - \frac{\theta_0^5}{512\pi}. \quad (17)$$

This approximation differs from the correct value of λ by no more than 0.0035 over the entire range $\theta_0 \in (0, \pi)$, and is accurate to within 3% over the range $\theta_0 \in (0, 3.1)$ radians.

The notch stress intensity factor will be determined by the sample geometry and the loading conditions a long way from the notch. In particular, for a notch with a length scale of L_{cr}, where the tensional stress field a long way from the tip is σ_∞, we see on dimensional grounds that

$$K_I^N \propto \sigma_\infty L_{cr}^\lambda. \quad (18)$$

Considering the case of $\theta_0 = 0$ (a 'crack' in Griffith's sense) the notch stress intensity factor is called simply the 'stress intensity factor' and written K_I [31]. There is then a critical value of this quantity, written K_{Ic}, above which the crack will grow. K_{Ic} is known as the 'critical stress intensity factor' or 'fracture toughness', and is usually considered a property of the material, independent of the loading geometry (although in Irwin's formulation, it is G which is the geometry-independent quantity). Irwin [32] showed that for

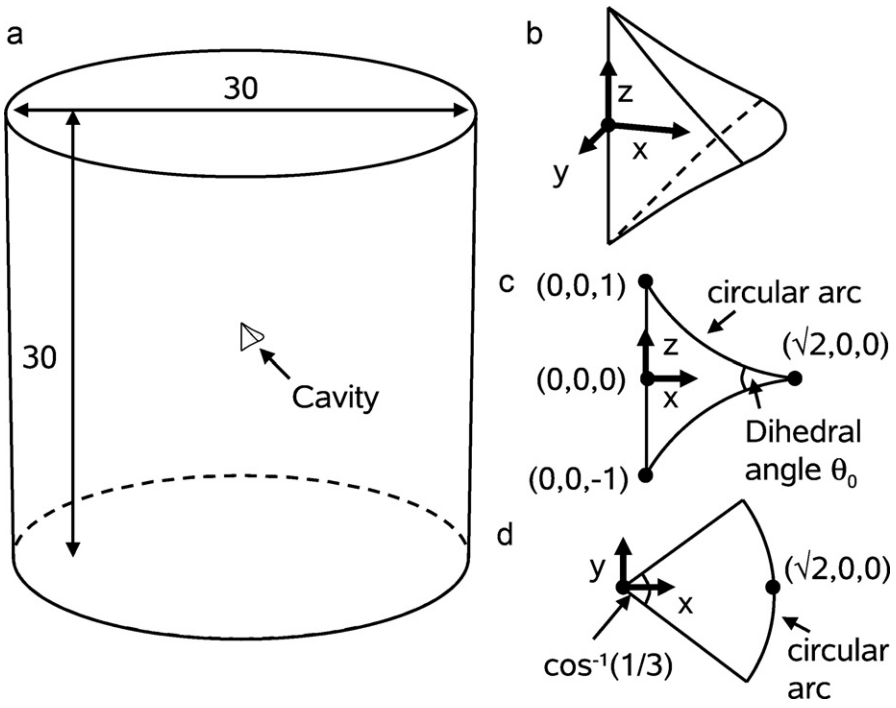

Fig. 6. Geometry of the elastic block and cavity used in the finite element simulations to calculate K_I^N in terms of applied stress. The cavity is intended as an approximation to the true cavity geometry of Fig. 4, and the stress divergence is studied numerically along the x-axis, near $x = \sqrt{2}$.

the case of plane stress (which is often the geometry used for measurements) $K_{Ic} = \sqrt{GE}$, which can be understood qualitatively by combining Eq. (18) (in the case $\lambda = 1/2$) with Eq. (14).

For notches, Seweryn (whom we follow here) [34] proceeds differently, by assuming that there are two geometry-independent material properties: an ultimate material strength for a single crystal under tension, termed $\sigma_{\max}$, and a characteristic length below which the assumption of continuum linear elasticity breaks down, which we denote ρ_c (and which in ideal cases might be as small as a couple of atomic spacings). For the analysis of this paper to be valid, ρ_c should be smaller than the grain size. In other words, the grain size should be sufficiently large that fracture is brittle.

The criterion suggested in Refs. [34,35] is that a crack propagates from the tip of a V-notch, when

$$\max\left(\int_0^{\rho_c} \sigma_\theta \, dr\right) \geq \rho_c \sigma_{\max}, \tag{19}$$

where the integral is taken along a ray perpendicular to the apex line of the notch, σ_θ is the stress component normal to the crack

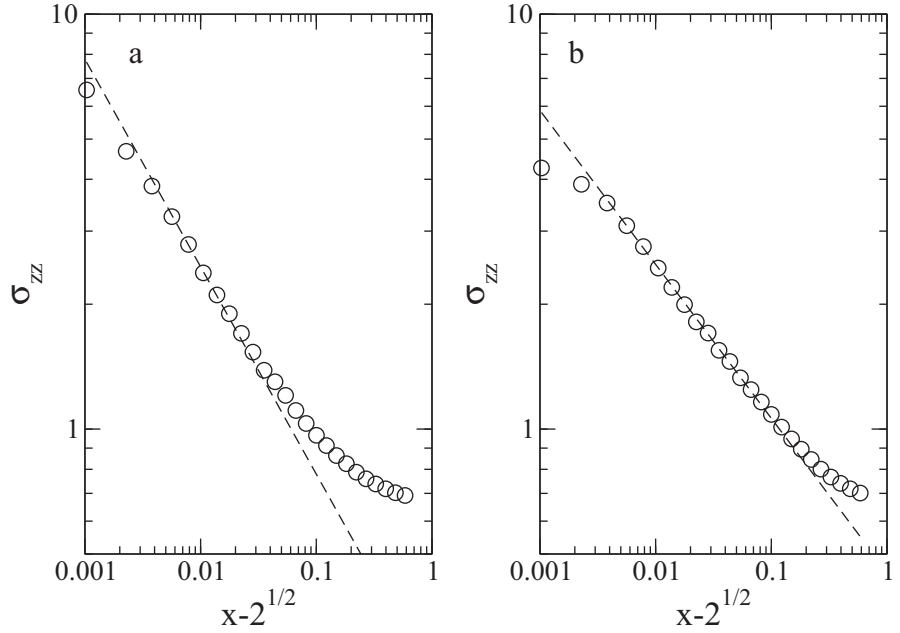

Fig. 7. Stress σ_{zz} versus $x - \sqrt{2}$ curves along the x-axis (symbols) together with a power law fit (dashed line) to the known power $-\lambda$ of Eq. (16). Panel (a) shows $\theta_0 = 0$, so $t = 2^{-1/2}$ and $\lambda = 0.5$, while (b) shows $\theta_0 = 2.158$ radians, so $t = -1$ and $\lambda = 0.371$. In both cases, the Poisson ratio is $\nu = 0.2$.

direction [so given asymptotically by Eq. (15) in our case] and the maximum is taken over all rays.

Applying the integral of Eq. (19), it is found [34] that a crack propagates if K_I^N from Eq. (15) satisfies

$$K_I^N \geq (1-\lambda)(2\pi\rho_c)^{\lambda}\sigma_{\max}. \tag{20}$$

In concept, this approach is slightly problematic, since the integral of Eq. (19) is performed in the region where the form of the stress being used is assumed to no longer be valid. However, the resulting criterion is simple, unambiguous, and agrees with the known limits for $\theta_0 = 0$ and π. Furthermore, the qualitative link back to Griffith's work is clear, because if a material behaves in this way, then the energy G required to create unit area of fracture surface should be of order $\sigma_{\max}^2\rho_c/E$. Thus, in the case of a crack, the Griffith criterion of Eq. (14) is recovered by means of Eqs. (18) and (20).

Consider Eq. (20). It is reasonable to expect experimental data to exist for the ultimate tensile stress of a single crystal; for example Seweryn approximates $\sigma_{\max}$ by single crystal yield stresses and quotes values of 240 MPa, 900 MPa and 800 MPa for low carbon steel, titanium alloy and toughened chromium–molybdenum steel respectively [34]. However the quantity ρ_c has not been widely measured. Therefore, in order to re-cast Eq. (20) in terms of more conventional quantities, we use the limit $\theta_0 = 0$ to re-write it in terms of K_{Ic}, the fracture toughness for a system in plane stress. The final result is that a crack will propagate if

$$K_I^N \geq (1-\lambda)(2K_{Ic})^{2\lambda}(\sigma_{\max})^{1-2\lambda}, \tag{21}$$

and this is the criterion we use in what follows. Seweryn quotes values for K_{Ic} of 25 MPa$\sqrt{\text{m}}$, 84 MPa$\sqrt{\text{m}}$ and 65 MPa$\sqrt{\text{m}}$, respectively for the three materials just mentioned.

In order to complete our analysis, we need to relate the applied stress σ_∞ for our complex tetrahedral cavities, to the notch stress intensity factor K_I^N at their edges. This requires a set of finite element calculations, since the geometries are too complex to be tractable analytically.

In fact, we simplify the geometries of Fig. 4 slightly in order to facilitate meshing. The simulations are conducted using a cylindrical block of isotropic elastic material, centred at the origin of coordinates, and with its axis parallel to the z-axis (Fig. 6). The length and diameter of the cylinder are each 30 units. From the centre of this material, we remove a cavity, with the following form: take a two dimensional curved triangular shape, with one straight edge of length 2 coincident with the z-axis. The other two sides are circular arcs, with radii $[3t^2 + (3/4)]^{1/2}$, where t is a parameter setting the notch angle at the outer edge via

$$\theta_0 = \pi - 2\tan^{-1}\left(\frac{2t\sqrt{2}+1}{2t-\sqrt{2}}\right), \tag{22}$$

and the centres of the arcs are given by

$$(x, y, z) = \left[2^{-1/2} + t, 0, \pm(2^{-1} + 2^{1/2}t)\right]. \tag{23}$$

The two-dimensional shape is then rotated around the z-axis, sweeping out a total angle of $\cos^{-1}(1/3)$ in order to form our approximation to the tetrahedral cavity, which has $z = 0$ and $y = 0$ as planes of reflection symmetry. Under this construction, the vertices of the cavity coincide with those of a regular tetrahedron, and the effective crack length is $L_{cr} = \sqrt{2}$ units.

The two flat surfaces of the cylinder are given a fixed displacement of $\pm 10^{-3}$ units in the z-direction (so the strain is 6.67×10^{-5}) and the material is arbitrarily given an elastic modulus of $E = 10^4$ units (so $\sigma_\infty \approx 6.67 \times 10^{-1}$ units). Three different values of Poisson ratio $\nu = 0.2$, 0.3 and 0.4 are used.

The finite element meshes contain between 11 400 and 12 000 nodes, and between 59 000 and 62 000 elements. The geometry is finely meshed in the neighbourhood of the notch tip, concentrating the most part of the elements there in order to more accurately capture the stress distribution ahead of this line. The elements used are 'Abaqus' [36] 4-node tetrahedral elements (C3D4). In the neighbourhood of the notch tip along the x-axis ($x \gtrsim \sqrt{2}$) the stress component σ_{zz} is recorded, and where it displays a power-law behaviour, this is fitted to Eq. (15)

$$\sigma_{zz} = \frac{K_I^N}{\left[2\pi\left(x-\sqrt{2}\right)\right]^{\lambda}} \equiv \sigma_\infty \frac{P(\theta_0,\nu)L_{cr}^{\lambda}}{\left[2\pi\left(x-\sqrt{2}\right)\right]^{\lambda}}, \tag{24}$$

using the known value of λ from Eq. (16). In this expression, we have used Eq. (18) to define a dimensionless function $P(\theta_0, \nu)$, which depends only on the notch angle and Poisson ratio.

Examples for a couple of notch angles are shown in Fig. 7, and values for $P(\theta_0, \nu)$ in Fig. 8.

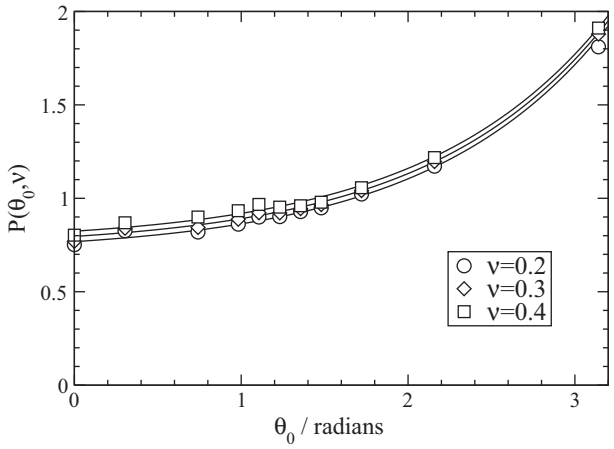

Fig. 8. Symbols: the quantity $P(\theta_0, \nu)$ obtained by fitting to finite element simulations. Lines: approximation to $P(\theta_0, \nu)$ from Eq. (25).

These data for $P(\theta_0, \nu)$ can be fitted to the approximate form

$$P(\theta_0, \nu) \approx 0.65 + 0.28\nu + 0.062\exp(0.93\theta_0), \tag{25}$$

where θ_0 is as usual measured in radians.

We are now in a position to relate the failure stress σ_F of the polycrystal (which is the value of σ_∞ at which a crack grows from the edge of a cavity) to the cavity size L_{cr}. This is done by combining Eq. (24) with Eq. (21), and gives:

$$\sigma_F = \frac{(1-\lambda)}{P(\theta_0,\nu)L_{cr}^{\lambda}}(2K_{Ic})^{2\lambda}(\sigma_{\max})^{1-2\lambda}, \tag{26}$$

where (to recap), $\sigma_{\max}$ is the ultimate tensile strength of a single crystal, and K_{Ic} is the fracture toughness of a single crystal.

5. Results and discussion

Consider now the foam-like structure described in Section 2, which forms an approximation to our polycrystalline material. If this material contains a volume fraction ϕ of voids (with the geometry described in Section 3) and ϕ is sufficiently small that the voids around the tetrahedral vertices (Fig. 2) do not frequently overlap, then Eq. (8) allows us to construct an implicit equation for the effective crack length L_{cr} in the structure:

$$\phi = A(\theta_0)L_{cr}^3\frac{n_V}{\langle V\rangle} + B(\theta_0)L_{cr}^2\frac{l_E}{\langle V\rangle^{2/3}}. \tag{27}$$

Our final result consists in taking Eq. (27) and then using Eqs. (5) and (7) to eliminate n_V and l_E in favour of the polydispersity parameter p; also Eqs. (10)–(13) to express A and B in terms of θ_0 (in radians), Eq. (17) to approximate λ and Eqs. (25) and (26) to eliminate L_{cr} in favour of σ_F and material properties K_{Ic} and $\sigma_{\max}$ of the

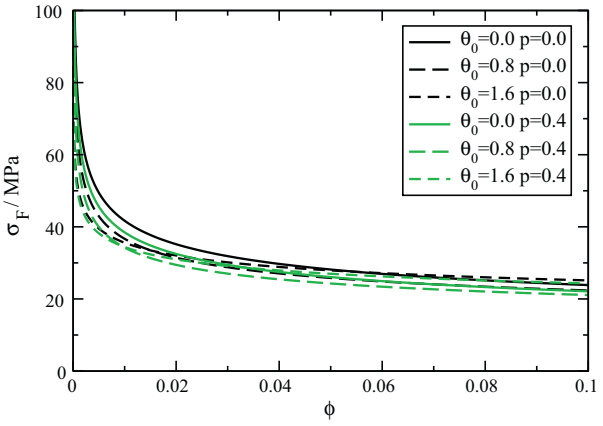

Fig. 9. Example calculation of σ_F versus ϕ, using $K_{Ic} = 100\,\mathrm{kPa}\sqrt{\mathrm{m}}$, $\sigma_{\max} = 1\,\mathrm{GPa}$, $\nu = 0.25$ and $\langle V \rangle = 10^{-12}\,\mathrm{m}^3$. Results for different values of θ_0 and p are plotted.

crystals. The result is an implicit relationship between the failure stress and various parameters of the polycrystal, such as the volume fraction, polydispersity, grain size and dihedral angle. Inverting the expression to obtain an explicit formula for σ_F requires solving a cubic equation with one positive real root, which can be done using standard methods [37], but for plotting the results, the implicit form is equally useful.

Fig. 9 shows examples of σ_F versus ϕ, plotted for different values of θ_0 and p. The effect of θ_0 at different values of ϕ is somewhat complex, due to the non-trivial behaviour of $A(\theta_0)$ and $B(\theta_0)$. However, we see from Fig. 9 that in general, increasing polydispersity leads to a lowering of σ_F, provided other quantities are unchanged. There are two qualitative arguments to explain this effect: First, this can be seen as a packing effect, in that polydisperse objects in general pack more efficiently than monodisperse objects (see for example Ref. [38]). This leaves more void space available to form larger incipient cracks. Second, and even more simply, we can conceptually think of forming a polydisperse sample by merging sets of equal sized crystals. This again liberates void space which was between the now-merged crystals, and which can therefore increase the size of the remaining voids.

The calculation we have presented results in a general expression for the failure under tension of a polycrystal with void space provided the crystals are large enough to fracture in a brittle manner. However, other failure mechanisms will also be available, and may either dominate, or interact with the case analysed here. For example, stresses from elastic anisotropy may not only activate crack precursors (as analysed in Ref [16]) but may also enhance the stresses experienced by the notched cavities we have analysed here. Such highly inhomogeneous stresses may also mean that the dominant failure mechanism of the cavities is no longer mode I fracture, but may be mixed mode instead, which will require a modified analysis based on the changed stress divergences so produced [34].

Lastly, we note that our analysis applies to tensional failure. Under compression, more complex processes can operate: Coulomb friction between crack surfaces will hinder their growth; and other microstructural phenomena, such as the formation of wing cracks and crack combs [39] may occur in the lead-up to ultimate material failure.

Acknowledgements

The authors wish to thank Javier Aldazabal, José Manuel Martínez-Esnaola and Antonio Martín-Meizoso of CEIT and Tecnun (University of Navarra) for useful discussions, and an anonymous reviewer for valuable suggestions.

Appendix A. Calculating shapes of voids

Suppose that the void is centred at the origin. We define four unit vectors, lying in the directions of the plateau borders:

$$\hat{\mathbf{n}}_0 = (0, 0, -1)^T, \tag{A.1}$$

$$\hat{\mathbf{n}}_1 = (2\sqrt{2}/3, 0, 1/3)^T, \tag{A.2}$$

$$\hat{\mathbf{n}}_2 = (-\sqrt{2}/3, \sqrt{2/3}, 1/3)^T, \tag{A.3}$$

$$\hat{\mathbf{n}}_3 = (-\sqrt{2}/3, -\sqrt{2/3}, 1/3)^T. \tag{A.4}$$

Furthermore, let us define two more unit vectors, which together with $\mathbf{n}_1$ form an orthonormal set:

$$\hat{\mathbf{n}}_{1a} = (-1/3, 0, 2\sqrt{2}/3)^T, \tag{A.5}$$

$$\hat{\mathbf{y}} = (0, 1, 0)^T. \tag{A.6}$$

A.1. Mesh geometry for open-ended voids

We choose the initial surface for the cavity in Fig. 2(a) to be represented by a mesh with the topology shown in Fig. 4(a) and (b).

In this figure, the cavity consists of four curved surfaces (which are open at their ends), and each of these surfaces is built from 6 symmetric pieces, of which one is shown shaded in Fig. 4(a).

The initial positions of the nodes in this shaded piece are given by the set $\{\mathbf{r}^{[0]}_{m,n}\}$, where $m \in \{0, \ldots, M\}$ and $n \in \{0, \ldots, N\}$. The integer n labels nodes outwards in the $\hat{\mathbf{n}}_1$ direction, and

$$\mathbf{r}^{[0]}_{m,n} \equiv \mathbf{s}_m + \frac{(N-n)\lambda_m}{N}\hat{\mathbf{n}}_1, \tag{A.7}$$

$$\lambda_m \equiv -\frac{\mathbf{s}_m \cdot \mathbf{v}}{\hat{\mathbf{n}}_1 \cdot \mathbf{v}}, \tag{A.8}$$

$$\mathbf{v} \equiv (\sqrt{3}/2, -1/2, 0)^T, \tag{A.9}$$

$$\mathbf{s}_m \equiv \frac{L\hat{\mathbf{n}}_1 + l_0\hat{\mathbf{n}}_{1a} + l_0 m\sqrt{3}\hat{\mathbf{y}}}{M}. \tag{A.10}$$

In these expressions, l_0 sets the distance of the initial (flat) portions of surface from the origin, and is arbitrary.

During optimization, we allow the nodes to move along predefined lines, so that the position of $\mathbf{r}_{m,n}$ of node (m, n) is defined through the scalar $q_{m,n}$ by

$$\mathbf{r}_{m,n} = \frac{nL}{N}\hat{\mathbf{n}}_1 + q_{m,n}\left[\mathbf{r}^{[0]}_{m,n} - \frac{nL}{N}\hat{\mathbf{n}}_1\right]. \tag{A.11}$$

To find the correct surface, we construct and minimize an energy functional, which (as described in Section 3) is the surface free energy of the shape, plus a Lagrange multiplier times the square of the difference between the actual cavity volume and a target volume. When the minimization is complete, we calculate the cavity volume v, and

$$L_{cr} = 2|\mathbf{r}_{M,0}|. \tag{A.12}$$

A.2. Mesh geometry for closed voids

We choose the initial surface for the cavity in Fig. 2(b) to be represented by a mesh with the topology shown in Fig. 4(c) and (d).

The initial positions of the nodes on one of the four symmetric surfaces lie on a regular tetrahedron, and have positions given by the set $\{\mathbf{r}^{[0]}_{m,n}\}$, where $m \in \{0, \ldots, N\}$ and $n \in \{0, \ldots, m\}$ and N is even. Specifically,

$$\mathbf{r}^{[0]}_{m,n} \equiv l_0\left(1 - \frac{m}{N} - \frac{n}{N}\right)\mathbf{n}_1 + l_0\left(\frac{m}{N}\right)\mathbf{n}_2 + l_0\left(\frac{n}{N}\right)\mathbf{n}_3. \tag{A.13}$$

In this expression, l_0 sets the distance of the initial (flat) portions of surface from the origin, and is arbitrary.

During optimization, we allow the nodes to move along rays through the origin, so that the position of $\mathbf{r}_{m,n}$ of node (m, n) is defined through the scalar $q_{m,n}$ by

$$\mathbf{r}_{m,n} = q_{m,n}\mathbf{r}^{[0]}_{m,n}. \tag{A.14}$$

Optimization is performed as for the open cavities, and when it is complete, we calculate the cavity volume v, and

$$L_{cr} = 2|\mathbf{r}_{N/2,0}|. \tag{A.15}$$

References

[1] M.G. Best, Igneous and Metamorphic Petrology, 2nd ed., Wiley-Blackwell, 2002.
[2] P.R.F. Barnes, E.W. Wulff, J. Glaciol. 50 (2004) 311–324.
[3] D.L. Dorset, Acta Crystallogr. B 51 (1995) 1021–1028.
[4] R.M. German, Sintering Theory and Practice, Wiley-Interscience, 1996.
[5] K. van Malssen, A. van Langevelde, R. Peschar, H. Schenk, J. Am. Oil Chem. Soc. 76 (1999) 669–676.
[6] C. Clarke, The Science of Ice Cream. The Royal Society of Chemistry, 2004. ISBN 0854046291.
[7] E.O. Hall, Proc. Phys. Soc. Sect. B 64 (1951) 747–753.
[8] D. Hull, D.J. Bacon, Introduction to Dislocations, 4th ed., Elsevier Publishing, 2001.
[9] Z. Jiang, J. Lian, B. Baudelet, Acta Metall. Mater. 43 (1995) 3349–3360.
[10] A.N. Stroh, Adv. Phys. 6 (1957) 418–465.
[11] D.M. Cole, Cold Reg. Sci. Technol. 15 (1988) 79–87.
[12] L.W. Gold, Philos. Mag. A 26 (1972) 311–328.
[13] C.R. Picu, V. Gupta, J. Mech. Phys. Solids 45 (1997) 1495–1520.
[14] A.G. Evans, Acta Metall. 26 (1979) 1845–1853.
[15] R.C. Picu, V. Gupta, J. Appl. Mech. 63 (1996) 295–300.
[16] S. Shyam Sunder, M.S. Wu, Cold Reg. Sci. Technol. 18 (1990) 29–47.
[17] A.A. Griffith, Phil. Trans. Roy. Soc. Ser. A 221 (1921) 163–198.
[18] W.A. Edelstein, E.M. Schulson, J. Glaciol. 37 (1991) 177–180.
[19] M.J. Ohara, Nature 5602 (1977) 503–507.
[20] C. Coleou, et al., Ann. Glaciol. 32 (2001) 75–81.
[21] S. Shyam Sunder, S. Nanthikesan, Cold Reg. Sci. Technol. 18 (1990) 249–265.
[22] W.K. Burbon, N. Cabrera, F.C. Frank, Phil. Trans. R. Soc. Lond. 243 (1951) 299–358.
[23] H.J. Frost, M.F. Ashby, Deformation Mechanism Maps: The Plasticity and Creep of Metals and Ceramics, Pergamon Press, 1982, http://dartmouth.edu/defmech/.
[24] A. Karma, W.J. Rappel, Phys. Rev. E 57 (1998) 4323–4349.
[25] G. Wulff, Z. Krystallogr. 34 (1901) 449–530.
[26] W.W. Mullins, J. Appl. Phys. 28 (1957) 333–339.
[27] C.S. Smith, in: C. Herring (Ed.), Metal Interfaces, Americal Soc. for Metals, Cleveland, 1952.
[28] J. Plateau, Statique Expérimentale et Theorétique des Lipides Soumis aux Seules Forces Moléculaires, Gaitier-Villars, Paris, 1873.
[29] A.M. Kraynik, D.A. Reinelt, F. van Swol, Phys. Rev. Lett. 93 (2004) 208301.
[30] L. Euler, Novi Commun. Acad. Sci. Imp. Petropol. 4 (1752–3) 109.
[31] M. Janssen, Z. Zuidema, R. Wanhill, Fracture Mechanics, Spon Press, Taylor & Francis Group, 2002.
[32] G. Irwin, J. Appl. Mech. 24 (1957) 361–364.
[33] M.L. Williams, J. Appl. Mech. 19 (1952) 526–528.
[34] A. Seweryn, Eng. Fract. Mech. 47 (1994) 673–681.
[35] V.V. Novozhilov, Prikl. Mat. Mek. 33 (1969) 212.
[36] Abaqus FEA, from Dassault Systèmes (SIMULIA), http://www.simulia.com.
[37] H. Cardano, Artis Magnæ, Sive de Regulis Algebraicis. Liber Unus, 1545. Available in English translation as: T.R. Witmer, Ars Magna or the Rules of Algebra, Dover, 1993.
[38] R.S. Farr, R.D. Groot, J. Chem. Phys. 131 (2009) 244104.
[39] E.M. Schulson, Eng. Fract. Mech. 68 (2001) 1839–1887.